Journal of Applied Pharmaceutical Science Vol. 12(11), pp 010-020, November, 2022
Available online at http://www.japsonline.com
DOI: 10.7324/JAPS.2022.121102
ISSN 2231-3354

Discovery of novel trihybrids based on salicylic acid/isoleucine/N-acylhydrazone: A promising therapeutic opportunity in colorectal cancer

David Preciado, Gustavo Moreno, Wilson Cardona, Andres Felipe Yepes*
Chemistry of Colombian Plants, Institute of Chemistry, Faculty of Exact and Natural Sciences University of Antioquia-UdeA, Medellín, Colombia.

ARTICLE INFO

Received on: 08/04/2022
Accepted on: 04/07/2022
Available Online: 05/11/2022

Key words:
Colorectal cancer, salicylic acid, isoleucine, *N*-acylhydrazone, cytotoxicity, antiproliferative activity.

ABSTRACT

Twelve novel trihybrids bearing salicylic acid/isoleucine/*N*-acylhydrazone (SA-Ile-NAH) features were designed, synthetized, and evaluated for anti-colorectal cancer (CRC) effects against SW480 human colon adenocarcinoma cells. SA-Ile-NAH hybrids **4a–l** were obtained in moderate to excellent yields (54%–94%). Regarding biological results, trihybrids **4a**, **4c**, **4f**, and **4j** showed 2- to 8-fold higher cytotoxic activities after 48 hours of exposure than the standard chemotherapeutic 5-fluorouracil (5-FU) (174. 30 ± 19.10), with inhibitory concentration (IC_{50}) values of 20.43 ± 1.88 to 78.15 ± 6.73 µM, respectively. Of those, 2,5-dimethoxy-substituited trihybrid **4j** is highlighted for its antiproliferative response with viability below 11% in the low micromolar range after 8 days of treatment, as well as for having no significant toxic effects on nontumorigenic cells (IC_{50} = 102.40 ± 4.64; IS = 1.31) beyond 48 hours of treatment. Finally, theoretical drug-likeness studies suggest that the promising **4j** exhibits optimal biopharmaceutical indices. From a therapeutic perspective, merging key pharmacophoric features of SA-Ile-NAH provides a new medicinal scaffold for developing new chemopreventive agents against CRC.

INTRODUCTION

Cancer is the leading cause of death worldwide, accounting for nearly 10 million deaths in 2020, or nearly 1 in 6 deaths. It is estimated that the number of deaths may increase up to 28.4 million in 2040. Female breast cancer has surpassed lung cancer as the most commonly diagnosed cancer, with an estimated 2.3 million new cases (11.7%), followed by lung (11.4%), colorectal (10.0%), prostate (7.3%), and stomach (5.6%) cancers (Ferlay *et al*., 2020; Sung *et al*., 2021). Packages of effective and resource-sensitive preventative and therapeutic interventions are available for cancer; however, serious side effects, resistance, and long-term sequelae offered by these modern treatments continue to be major problems in cancer therapies. To date, colorectal cancer (CRC) is the third most deadly and fourth most commonly diagnosed cancer in the world. In fact, CRC is the third leading cause of cancer death in both men and women, and the second overall among men and women combined (GLOBOCAN, 2021; Høydahl *et al*., 2020; Siegel *et al*., 2021). Because standard treatments for CRC usually involves surgery to remove the cancer tumor, followed by adjuvant chemotherapy or radiation therapy, and because of the high toxicity associated with standard chemotherapy regimens together with drug resistance, high doses, and low tumor-specific selectivity, there is an urgent need to search for novel, more potent, safe, and selective treatment strategies in CRC based on targeted therapies able to interfere with closely related signaling pathways in CRC.

Marketed by Bayer under the trade name Aspirin, acetylsalicylic acid (ASA) used currently for minor pain relief and fever reduction has also demonstrated to have chemopreventive effects in cancer incidence and mortality associated with CRC (Bagheri *et al*., 2018; Burn *et al*., 2020; Cuzick *et al*., 2009; Patrignani and Patrono, 2016; Peleg *et al*., 1994; Spiegel, 2020;

*Corresponding Author
Andres Felipe Yepes, Medellín, Colombia., Chemistry of Colombian Plants, Institute of Chemistry, Faculty of Exact and Natural Sciences University of Antioquia-UdeA, Medellín, Colombia
E-mail: andresf.yepes @ udea.edu.co

Thun *et al*., 1991). As for ASA, its metabolite salicylic acid (SA), displayed antiproliferative and proapoptotic effects in CRC in *in vitro* and *in vivo* models (Brennan *et al*., 2021; Deb *et al*., 2011; Elder *et al*., 1996; Elder and Paraskeva 1999; Giardina and Inan, 1998; Gökçe *et al*., 2017; Pathi *et al*., 2012; Paterson and Lawrence, 2001). Similarly, isoleucine has been revealed to exhibit high potency against several cancer cell lines, including lines of human colorectal carcinoma cells (Ananieva and Wilkinson, 2018; Lieu *et al*., 2020; Murata *et al*., 2007; Wakshlag *et al*., 2006). Furthermore, reports of diagnosed CRC patients suggest that isoleucine is linked to survival after diagnosis. This finding not only suggests isoleucine as a possible prognostic biomarker in CRC patients, but that those patients might need more of this amino acid (Bener *et al*., 2006; Delphan *et al*., 2018; Long *et al*., 2020; Wang *et al*., 1997). In addition, the antitumoral effectiveness of *N*-acylhydrazone-containing compounds, especially to prevent proliferation in human colorectal cancerous cells, has been extensively reported (Al-awar *et al*., 2019; Dasgupta *et al*., 2020; Huff *et al*., 2018; Iliev *et al*., 2019; Song *et al*., 2011; Thota *et al*., 2018). In this regard, *N*-acylhydrazones derivatives have drawn special attention for anticancer treatment, due to their ability for inhibiting the growth of a range of tumor cells including lung, colon, pancreas, and breast cancer, at micromolar levels (Buss *et al*., 2002; Chen *et al*., 2018; Chaston *et al*., 2003).

From a therapeutic point of view, due to the complexity of cancer and the abnormal activation of several signaling pathways in its progression, the multitarget-directed ligands strategy is considered to be an effective way to treat this disease. In an extension to this approach, merging of two (or more than two) antitumoral pharmacophoric features from known bioactive compounds covalently linked to a single molecule (hybrid molecules) offers new avenues for the development of improved chemotherapeutic cancer candidates (Ali *et al*., 2013; Viegas-Junior *et al*., 2007). Thus, considering the high antitumoral effectiveness found for SA, isoleucine and the *N*-acylhydrazone have not been combined into a single drug candidate for anticancer agent, and so we designed for the first time a series of molecular hybrids featuring structurally moieties of SA, *N*-acylhydrazone, and isoleucine into parent molecules (Fig. 1). To further analyze their structure–activity relationships (SARs), the phenyl ring substitution on *N*-acylhydrazone framework was used. We hypothesize that these new hybrids would exert a valuable antitumor response, in a synergistic effect, leading to tumor cell apoptosis in human colon carcinoma SW480 cells, which would likely open a new clinical possibility for CRC management. The most promising hybrid was also chosen to be investigated for its pharmacokinetics profile using *in silico*-derived parameters.

MATERIALS AND METHODS

General information

All chemicals used were obtained from commercial suppliers and used without further purification. Thin-layer chromatography (TLC, silica gel 60 F254) was used to follow reactions and was visualized in an iodine chamber or with a UV lamp (λ = 254 nm). Melting points were determined using a Stuart SMP10 Digital Melting Point instrument. Microwave-assisted reactions were conducted in CEM Focused Microwave. Nuclear Magnetic Spectroscopy (NMR) spectra of compounds measured on a Varian instrument spectrometer (300 MHz ^{1}H NMR and 75 MHz ^{13}C NMR), ^{1}H and ^{13}C NMR spectra were recorded in DMSO-d_6, $CDCl_3$, or CD_3OD solutions and chemical shift values are in parts per million (ppm) using the Me_4Si as internal standard.

Preparation of methylisoleucinate (1)

Thionyl chloride (1.5 mmol) was dissolved into dry methanol (10 ml) cooled to −10°C and the resulting mixture was stirred for 5 minutes. Afterward, the solution was treated with isoleucine (1.0 mmol), stirred for 10 minutes, maintained at −10°C for 2 hours, and then kept at room temperature for another 24 hours. After completion of the reaction, the reaction mixture was poured into ether (100 ml) and cooled for 2 hours collecting the

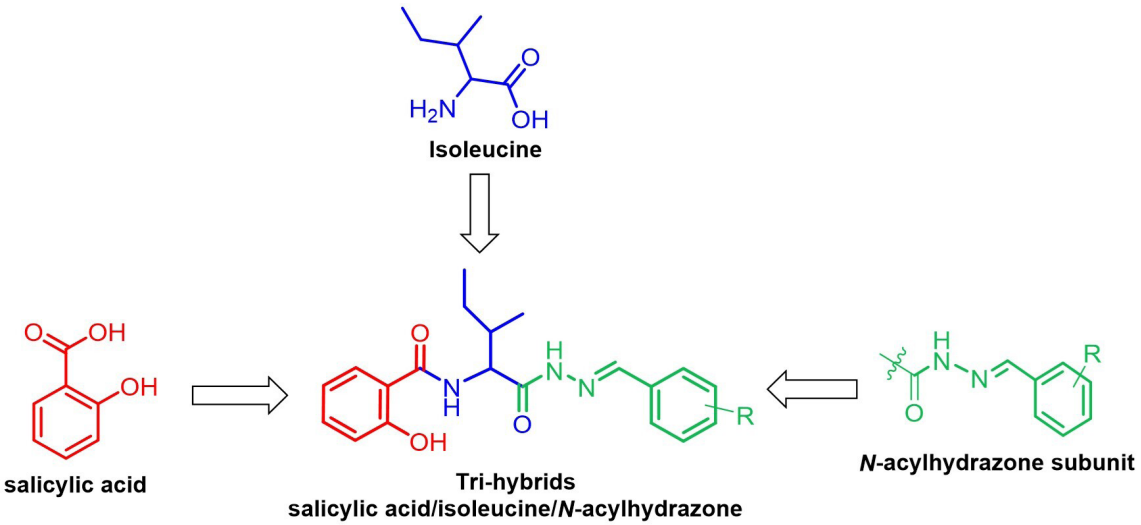

Figure 1. Design strategy of the novel trihybrids bearing salicylic acid (in red), isoleucine (in blue), and N-acylhydrazone (in green) features as anticancer agents.

interfacial precipitate which was filtered and oven-dried at 45°C for 24 hours; pure product **1** was obtained in a quantitatively yield (95%) as colorless needles: mp 96°C–98°C. ^{1}H NMR (300 MHz, $CDCl_3$) δ 3.90 (dd, *J* = 10.2, 4.2 Hz, 1H), 3.74 (s, 1H, CH_3O), 1.67–1.39 (m, 1H), 1.34–1.03 (m, 1H), 0.94 (d, *J* = 6.9 Hz, 3H, CH_3), 0.92 (t, *J* = 8.0 Hz, 3H, CH_3). ^{13}C NMR (75 MHz, $CDCl_3$) δ 168.9 (C=O), 56.8 (CH-NH), 52.2 (CH_3O), 36.4 (CH), 25.3 (CH_2), 13.5 (CH_3), 10.6 (CH_3).

Synthesis of methyl (2-hydroxybenzoyl)isoleucinate (2)

The present synthetic procedure is similar to a previously reported method (Castrillón *et al*., 2019). Triethylamine (4 mmol) and SA (1 mmol) in Tetrahydrofuran (THF) (10 ml) were stirred for 15 minutes. 2-(1H-benzotriazol-1-yl)-1,1,3,3-tetramethyluronium hexafluorophosphate, Hexafluorophosphate Benzotriazole Tetramethyl Uronium (HBTU) (1.5 mmol) was added to this mixture and stirred for a further 20 minutes. Isoleucine ester **1** (1.2 mmol) was then added and allowed to stir for 24 hours. Upon completion, the reaction mixture solvent was evaporated to dryness under reduced pressure and the residue was purified on a silica gel chromatography using mixtures hexane-ethyl acetate (1:1 ratio) as eluent yielding pure intermediate **2** in a good yield (71%) as a viscous yellow oil. ^{1}H NMR (300 MHz, $CDCl_3$) δ 7.46 (d, *J* = 8.2 Hz, 1H, 1-H), 7.40 (t, *J* = 8.2 Hz, 1H, 3-H), 6.98 (d, *J* = 8.2 Hz, 1H, 4-H), 6.88 (t, *J* = 8.2 Hz, 1H, 2-H), 4.78 (dd, *J* = 8.3, 4.9 Hz, 1H), 3.79 (s, 3H, OCH_3), 2.13–1.90 (m, 1H), 1.64–1.36 (m, 1H), 1.39–1.05 (m, 1H), 1.07–0.82 (m, 6H, 2 × CH_3). ^{13}C NMR (75 MHz, DMSO-d_6) δ 172.3 (C=O), 169.6 (C=O), 161.6 (Ar-O), 134.6 (Ar), 125.6 (Ar), 118.8 (Ar), 118.7 (Ar), 114.0 (Ar), 55.4 (CH-NH), 52.6 (CH_3O), 38.2 (CH), 25.4 (CH_2), 14.8 (CH_3), 11.8 (CH_3).

Synthesis of N-((2S,3S)-1-hydrazineyl-3-methyl-1-oxopentan-2-yl)-2-hydroxybenzamide (3)

The present synthetic procedure is similar to a previously reported method (Coa *et al*., 2015; Vergara *et al*., 2017). Compound **2** (1 mmol) and MeOH (1 ml) were mixed. Subsequently, hydrazine hydrate (5 mmol, 98% solution) was added and the resulting mixture was stirred in a preheated oil bath at 65°C for 24 hours when analysis by TLC indicated the end of the reaction. After being cooled to room temperature, the solvent was evaporated under reduced pressure and the residue was poured onto ice. The resulting precipitate was filtered, washed with ice water, and oven-dried at 45°C for 24 hours, affording the corresponding *N*-acylhydrazide **3** as a white solid (93%); mp 111°C–113°C. ^{1}H NMR (300 MHz, Methanol-d_4) δ 7.90 (td, *J* = 8.0, 1.8 Hz, 1H), 7.38 (td, *J* = 8.0, 7.4, 1.8 Hz, 1H), 6.92 (m, 2H), 3.33 (dd, *J* = 8.1, 3.9 Hz, 1H), 2.10–1.92 (m, 1H), 1.70–1.44 (m, 1H), 1.04–0.92 (m, 6H, 2 × CH_3). ^{13}C NMR (75 MHz, Methanol-d_4) δ 171.7 (C=O), 168.1 (C=O), 158.3 (Ar-O), 133.4 (Ar), 129.0 (Ar), 119.0 (Ar), 116.7 (Ar), 116.5 (Ar), 56.6 (CH-NH), 36.8 (CH), 24.8 (CH_2), 14.5 (CH_3), 9.9 (CH_3).

General procedure for synthesis of trihybrids (4a–l)

The present synthetic procedure is similar to a previously reported method (Coa *et al*., 2015; Vergara *et al*., 2017). The appropriate aromatic aldehyde (1 mmol), acylhydrazide **3** (1 mmol), and a few drops of acetic acid in ethanol were deposited into a CEM microwave reaction vessel. After that, the mixture was irradiated in a CEM Discover microwave synthesizer at 200 W in the open-vessel mode attached to a reflux condenser at 80°C with vigorous stir during 10 minutes. After being cooled to room temperature, the solvent was evaporated under reduced pressure and the oily residue was purified by preparative TLC over silica gel 60 F 254 (Merck) using an mixture of hexane:AcOEt (10:8–1:1) as eluent, furnishing the target hybrids **4a–l** in the yields as described below.

2-hydroxy-N-(1-(2-((2-hydroxynaphthalen-1-yl) methylene)hydrazineyl)-3-methyl-1-oxopentan-2-yl)benzamide (**4a**). Pale yellow solid; yield = 94%; mp = 258°C–260°C; ^{1}H NMR (300 MHz, DMSO-d_6) δ 9.22 (s, 1H, N=C-H), 7.93–7.72 (m, 2H), 7.67–7.48 (m, 2H), 7.32 (t, *J* = 8.1 Hz, 1H), 7.14–7.00 (m, 2H), 6.85–6.66 (m, 2H), 6.42 (t, *J* = 7.8 Hz, 1H), 4.60 (d, *J* = 6.9 Hz, 1H), 2.06–1.92 (m, 1H), 1.70–1.43 (m, 2H), 1.06–0.71 (m, 6H, 2 × CH_3). ^{13}C NMR (75 MHz, DMSO-d_6) δ 172.7 (C=O), 168.2 (C=O), 159.2 (Ar-O), 157.2 (Ar-O), 140.6 (C=N), 137.4, 133.6, 132.6, 130.4, 129.1, 127.1, 126.8, 125.9, 124.3, 120.0, 118.8, 118.6, 117.4, 133.5, 56.6, 37.4, 25.1, 16.1 (CH_3), 11.4 (CH_3).

2-hydroxy-N-(1-(2-(2-hydroxybenzylidene)hydrazineyl)-3-methyl-1-oxopentan-2-yl)benzamide (**4b**). Pale yellow solid; yield = 75%; mp = 280°C–282°C; ^{1}H NMR (300 MHz, DMSO-d_6) δ 8.11 (s, 1H, N=C-H), 7.64 (d, *J* = 7.8 Hz, 1H), 7.29–6.77 (m, 4H), 6.56 (d, *J* = 8.2 Hz, 2H), 6.30 (t, *J* = 7.1 Hz, 1H), 4.40 (d, *J* = 6.8 Hz, 1H), 2.18–1.75 (m, 1H), 1.42–1.08 (m, 2H), 0.98–0.70 (m, 6H, 2 × CH_3). ^{13}C NMR (75 MHz, DMSO-d_6) δ 172.7 (C=O), 168.7 (C=O), 165.8 (Ar-O), 156.7 (Ar-O), 152.5 (C=N), 149.0, 138.2, 137.9, 133.7, 131.9, 118.3, 114.8, 106.1, 104.6, 102.2, 62.8, 37.7, 26.4, 15.9 (CH_3), 11.4 (CH_3).

N-(1-(2-(2,3-dihydroxybenzylidene)hydrazineyl)-3-methyl-1-oxopentan-2-yl)-2-hydroxy benzamide (**4c**). Pale yellow solid; yield = 58%; mp = 197°C–199°C; ^{1}H NMR (300 MHz, DMSO-d_6) δ 8.85 (s, 1H, N = C-H), 8.34 (d, *J* = 7.5 Hz, 1H), 7.87 (t, *J* = 7.5 Hz, 1H), 7.38 (t, *J* = 7.5 Hz, 1H), 7.06 (d, *J* = 8.1 Hz, 1H), 6.85 (d, *J* = 7.2 Hz, 1H), 6.81 (t, *J* = 7.2 Hz, 1H), 6.75 (d, *J* = 8.1 Hz, 1H), 4.48 (d, *J* = 7.1 Hz, 1H), 2.10–1.78 (m, 1H), 1.68–1.27 (m, 2H), 1.00–0.64 (m, 6H, 2 × CH_3). ^{13}C NMR (75 MHz, DMSO-d_6) δ 168.4 (C=O), 168.2 (C=O), 157.5 (Ar-O), 147.3 (Ar-O), 145.4 (Ar-O), 145.3 (C=N), 134.1, 130.1, 122.7, 121.1, 120.2, 120.0, 119.4, 118.7, 117.5, 56.7, 36.8, 24.9, 15.6 (CH_3), 11.2 (CH_3).

N-(1-(2-(2,4-dihydroxybenzylidene)hydrazineyl)-3-methyl-1-oxopentan-2-yl)-2-hydroxy benzamide (**4d**). Pale yellow solid; yield = 54%; mp = 196°C–198°C; ^{1}H NMR (300 MHz, DMSO-d_6) δ 8.00 (s, 1H, N = C-H), 7.67 (dt, *J* = 7.9, 2.4 Hz, 1H), 7.20 (m, 2H), 7.88 (t, *J* = 8.2 Hz, 1H, 2-H), 7.01 (d, *J* = 3.2 Hz, 1H), 6.66 (dd, *J* = 8.5, 3.2 Hz, 1H), 6.52 (t, *J* = 7.4 Hz, 1H), 6.09 (d, *J* = 8.5 Hz, 1H), 4.34 (d, *J* = 6.8 Hz, 1H), 2.16–1.86 (m, 1H), 1.43–1.14 (m, 2H), 0.93 (d, *J* = 7.4 Hz, 3H, CH_3), 0.83 (t, *J* = 7.6 Hz, 3H, CH_3). ^{13}C NMR (75 MHz, DMSO-d_6) δ 171.5 (C=O), 171.0 (C=O), 168.9 (Ar-O), 153.9 (Ar-O), 151.4 (Ar-O), 142.1 (C=N), 135.5, 134.1, 134.1, 129.6, 122.2, 122.1, 117.7, 114.2, 110.5, 57.2, 36.9, 24.7, 15.5 (CH_3), 11.2 (CH_3).

N-(1-(2-(2,5-dihydroxybenzylidene)hydrazineyl)-3-methyl-1-oxopentan-2-yl)-2-hydroxy benzamide (**4e**). Pale yellow solid; yield = 86%; mp = 201°C–203°C; ^{1}H NMR (300 MHz, DMSO-d_6) δ 8.24 (s, 1H, N=C-H) 7.73 (td, *J* = 7.3, 1.7 Hz, 1H), 7.26 (dd, *J* = 7.3, 2.4 Hz, 1H), 6.89 (d, *J* = 2.7 Hz, 1H), 6.84 (dd, *J* = 7.5, 1.7 Hz, 1H), 6.77 (d, *J* = 8.4 Hz, 1H), 6.73 (dd, *J* = 8.4, 2.7 Hz, 1H), 6.59 (t, *J* = 7.5 Hz, 1H), 4.41 (d, *J* = 6.6 Hz, 0H), 2.24–1.90 (m, 1H), 1.47–1.20 (m, 2H), 1.01 (d, *J* = 6.9 Hz, 3H), 0.89 (t, *J* = 7.1 Hz, 3H). ^{13}C NMR (75 MHz, DMSO-d_6) δ 172.8 (C=O), 168.7 (C=O), 165.7 (Ar-O), 155.1 (Ar-O), 150.2 (Ar-O),

145.6 (C=N), 133.0, 130.1, 120.5, 119.3, 118.3, 118.0, 117.7, 116.2, 115.9, 55.9, 37.1, 25.0, 15.9 (CH_3), 11.9 (CH_3).

N-(1-(2-(3,4-dihydroxybenzylidene)hydrazineyl)-3-methyl-1-oxopentan-2-yl)-2-hydroxy benzamide (**4f**). Yellow solid; yield = 64%; mp = 188°C–191°C; ^{1}H NMR (300 MHz, DMSO-d_6) δ 7.98 (s, 1H, N=C-H), 7.79 (t, *J* = 7.6 Hz, 1H), 7.36 (t, *J* = 7.6 Hz, 1H), 7.22 (s, 1H), 6.99 (d, *J* = 7.7 Hz, 1H), 6.96–6.85 (m, 2H), 6.78 (d, *J* = 7.7 Hz, 1H), 4.34 (d, *J* = 7.6 Hz, 1H), 1.93–1.79 (m, 1H), 1.36–1.06 (m, 2H), 0.88–0.78 (m, 6H). ^{13}C NMR (75 MHz, DMSO-d_6) δ 169.0 (C=O), 167.6 (C=O), 157.2 (Ar-O), 152.5 (Ar-O), 149.9 (Ar-O), 147.8 (C=N), 145.1, 134.4, 130.0, 125.7, 122.1, 117.3, 117.0, 116.0, 113.4, 57.1, 36.8, 24.9, 14.8 (CH_3), 10.7 (CH_3).

2-hydroxy-N-(3-methyl-1-oxo-1-(2-(2,3,4-trihydroxybenzylidene)hydrazineyl)pentan-2-yl) benzamide (**4g**). Yellow solid; yield = 68%; mp = 126°C–128°C; ^{1}H NMR (300 MHz, DMSO-d_6) δ 8.22 (s, 1H, N=C-H), 7.85 (d, *J* = 8.5 Hz, 1H), 7.37 (t, *J* = 7.7 Hz, 1H), 7.06–6.84 (m, 2H), 6.77 (dd, *J* = 8.5, 2.4 Hz, 1H), 6.40 (d, *J* = 8.7 Hz, 1H), 4.38 (d, *J* = 7.2 Hz, 1H), 1.96–1.71 (m, 1H), 1.43–1.07 (m, 2H), 0.94–0.73 (m, 6H, 2 × CH_3). ^{13}C NMR (75 MHz, DMSO-d_6) δ 168.1 (C=O), 168.0 (C=O), 157.4 (Ar-O), 157.1 (Ar-O), 151.1 (Ar-O), 148.8 (Ar-O), 147.2 (C=N), 132.6, 130.2, 122.4, 120.2, 117.5, 117.1, 111.0, 108.2, 56.9, 36.9, 25.0, 15.6 (CH_3), 10.9 (CH_3).

N-(1-(2-(2,3-dimethoxybenzylidene)hydrazineyl)-3-methyl-1-oxopentan-2-yl)-2-hydroxy benzamide (**4h**). Pale yellow solid; yield = 91%; mp = 118°C–120°C; ^{1}H NMR (300 MHz, DMSO-d_6) δ 8.55 (s, 1H, N=C-H), 8.32 (d, *J* = 7.6 Hz, 1H), 7.92 (t, *J* = 7.6 Hz, 1H), 7.44 (t, *J* = 7.6 Hz, 1H), 7.27 (m, 2H), 7.11 (m, 2H), 4.44 (d, *J* = 7.0 Hz, 1H), 3.79 (s, 3H, OMe), 3.78 (s, 3H, OMe), 2.05–1.91 (m, 1H), 1.65–1.40 (m, 2H), 1.02–0.88 (m, 6H, 2 × CH_3). ^{13}C NMR (75 MHz, DMSO-d_6). δ 166.9 (C=O), 166.7 (C=O), 161.2 (Ar-O), 153.2 (Ar-OMe), 153.1 (Ar-OMe), 148.3 (C=N), 143.0, 133.2, 130.4, 128.1, 124.8, 118.6, 118.2, 117.4, 114.4, 61.6 (CH_3O), 57.0 (CH_3O), 56.2, 37.1, 27.0, 16.0 (CH_3), 11.3 (CH_3).

N-(1-(2-(2,4-dimethoxybenzylidene)hydrazineyl)-3-methyl-1-oxopentan-2-yl)-2-hydroxy benzamide (**4i**). Pale yellow solid; yield = 61%; mp = 120°C–122°C; ^{1}H NMR (300 MHz, DMSO-d_6) δ 8.52 (s, 1H, N=C-H), 7.91 (d, *J* = 8.1 Hz, 1H), 7.76 (dd, *J* = 8.6, 2.2 Hz, 1H), 7.74 (d, *J* = 8.4 Hz, 1H), 6.97 (t, *J* = 8.1 Hz, 1H), 6.93 (d, *J* = 7.7 Hz, 1H), 6.75 (d, *J* = 2.1 Hz, 1H), 6.65 (dd, *J* = 8.4, 2.1 Hz, 1H), 3.88 (d, *J* = 6.8 Hz, 1H), 3.85 (s, 3H, OMe), 3.82 (s, 3H OMe), 2.07–1.91 (m, 1H), 1.65–1.38 (m, 2H), 0.94 (d, *J* = 6.8 Hz, 3H), 0.89 (t, *J* = 7.2 Hz, 3H). ^{13}C NMR (75 MHz, DMSO-d_6) δ 167.9 (C=O), 167.4 (C=O), 162.9 (Ar-O), 159.5 (Ar-OMe), 159.4(Ar-OMe), 143.1 (C=N), 133.3, 130.4, 127.1, 118.4, 118.3, 115.5, 115.3, 106.8, 98.7, 56.2 (CH_3O), 56.1 (CH_3O), 55.9, 37.3, 27.0, 15.9 (CH_3), 11.4 (CH_3).

N-(1-(2-(2,5-dimethoxybenzylidene)hydrazineyl)-3-methyl-1-oxopentan-2-yl)-2-hydroxy benzamide (**4j**). Pale yellow solid; yield = 60%; mp = 127°C–129°C; ^{1}H NMR (300 MHz, DMSO-d_6) δ 8.59 (s, 1H, N=C-H), 8.33 (d, *J* = 7.5 Hz, 1H), 7.89 (d, *J* = 7.5 Hz, 1H), 7.32 (d, *J* = 3.1 Hz, 1H), 7.04 (d, *J* = 8.9 Hz, 2H), 7.00 (td, *J* = 8.6, 2.9 Hz, 1H), 6.92 (d, *J* = 8.6 Hz, 1H), 3.81 (s, 3H, OMe), 3.76 (d, *J* = 6.9 Hz, 1H), 3.74 (s, 3H, OMe), 2.07–1.89 (m, 1H), 1.65–1.39 (m, 2H), 0.97–0.87 (m, 6H, 2 × CH_3). ^{13}C NMR (75 MHz, DMSO-d_6) δ 168.3 (C=O), 167.4 (C=O), 153.7 (Ar-O), 152.7 (Ar-OMe), 152.4 (Ar-OMe), 142.9 (C=N), 133.1, 130.2, 123.2, 118.7, 118.4, 118.2, 117.4, 113.8, 109.4, 56.7 (CH_3O), 55.9 (CH_3O), 55.7, 37.2, 25.2, 16.0 (CH_3), 11.4 (CH_3).

N-(1-(2-(3,4-dimethoxybenzylidene)hydrazineyl)-3-methyl-1-oxopentan-2-yl)-2-hydroxy benzamide (**4k**). White solid; yield = 60%; mp = 108°C–110°C; ^{1}H NMR (300 MHz, DMSO-d_6) δ 8.18 (s, 1H, N=C-H), 7.96 (dd, *J* = 8.3, 1.4 Hz, 1H), 7.39–7.25 (m, 1H), 7.17 (dd, *J* = 7.5, 2.1 Hz, 1H), 7.01 (t, *J* = 8.3 Hz, 1H), 6.96 (dd, *J* = 7.5, 2.1 Hz, 1H), 6.83 (t, *J* = 7.5 Hz, 1H), 4.44 (d, *J* = 7.4 Hz, 1H), 3.79 (s, 6H, 2 × OCH_3), 2.07–1.90 (m, 1H), 1.67–1.34 (m, 1H), 1.02–0.74 (m, 6H, 2 × CH_3). ^{13}C NMR (75 MHz, DMSO-d_6) δ 173.1 (C=O), 173.0 (C=O), 168.0 (Ar-O), 167.4 (Ar-OMe), 166.5 (Ar-OMe), 151.1 (C=N), 149.4, 147.9, 127.3, 122.4, 118.5, 118.0, 117.4, 111.8, 108.6, 57.0 (CH_3O), 56.0 (CH_3O), 55.9, 37.0, 25.2, 15.9 (CH_3), 11.3 (CH_3).

2-hydroxy-N-(1-(2-((3-hydroxy-5-(hydroxymethyl)-2-methylpyridin-4-yl)methylene) hydrazineyl)-3-methyl-1-oxopentan-2-yl)benzamide (**4l**). Yellow solid; yield = 86%; mp = 198°C–200°C; ^{1}H NMR (300 MHz, DMSO-d_6) δ 8.64 (s, 1H, N=C-H), 7.77 (d, *J* = 7.8 Hz, 1H), 7.19 (s, 1H, H pyridine), 7.09 (t, *J* = 8.0 Hz, 1H), 6.75 (d, *J* = 8.1 Hz, 1H), 6.43 (d, *J* = 8.0 Hz, 1H), 4.46 (s, 2H, CH_2O), 4.44 (d, *J* = 6.9 Hz, 1H), 2.29 (s, 3H, CH_3-Py), 2.01–1.87 (m, 1H), 1.54–1.25 (m, 2H), 0.99 (d, *J* = 6.5 Hz, 3H), 0.93 (t, *J* = 7.4 Hz, 3H). ^{13}C NMR (75 MHz, DMSO-d_6) δ 168.0 (C=O), 166.2 (C=O), 158.3 (Ar-O), 154.1 (Py-O), 150.2 (Py-CH_3), 146.8 (C=N), 139.3 (C=N_{py}), 133.8, 132.6, 130.4, 128.9, 120.2, 118.5, 118.2, 68.6 (-CH_2O-Py), 60.2, 37.5, 25.1, 16.0 (CH_3-Py), 15.5 (CH_3), 11.3 (CH_3).

Biological activity assays

Cell lines and culture medium

Nonmalignant cells (CHO-K1) along with the adenocarcinoma colon cancer cell line (SW480) were used for biological experiments. Cultures were obtained from The European Collection of Authenticated Cell Cultures (England), cultivated with horse serum, 1% nonessential amino acids (Gibco Invitrogen, Carlsbad, CA), 10% heat-inactivated (56°C), and maintained in Dulbecco's Modified Eagle Medium. Serum was reduced to 3% and the medium was supplemented with insulin (10 mg/ml), selenium (5 ng/ml), and transferrin (5 mg/ml) (Herrera *et al*., 2018).

Cytotoxic activity

The colorimetric sulforhodamine B (SRB) assay was used to evaluate the cytotoxicity activity of the synthesized trihybrids as well as the reference compounds. Using 96-well tissue culture plates, cells were plated at a seeding density of 20,000 cells/well at 37°C and incubated in a humidified atmosphere containing 5% CO_2. All cultures were allowed to grow for 24 hours, and then treated with vehicle control containing 1% (v/v) DMSO or increasing concentrations (0.01–200 μM) of the target trihybrids, as well 5-FU (the standard drug), pyridoxal isonicotinoyl hydrazone (PIH), parental compounds (SA and isoleucine), and the equimolar mixture of these. After cell fixation with trichloroacetic acid (50% v/v, 1 hour at 4°C) (Merck), cell proteins were determined by staining with 0.4% (w/v) SRB (Sigma-Aldrich, United States), and afterward unbound SRB was removed washed with 1% acetic acid and left for air-drying. After that, 10 mM Tris base was used to dissolve protein-bound SRB. The absorbance measured at 492

nm in a microplate reader (Mindray MR-96A) (Perez *et al*., 2014). All experiments were conducted at least three times.

Antiproliferative ativity

The assessment of antiproliferative activity of the most promising compound was also tested through SRB assay. Typically, after the cells were seeded at an initial density of 2,500 cells/well in 96-well tissue culture plates, they were incubated in the same conditions described earlier for cytotoxicity. Afterward, cultures were allowed to grow for a period of 24 hours and then treated with DMSO (vehicle control, 1%) or increasing concentrations of the hit-trihybrid **4j** [6.25–100 µM, ranges dependent on the inhibitory concentration (IC_{50}) values] for 0, 2, 4, 6, and 8 days. The culture medium is changed every 48 hours. After the incubation time, cells were fixed, stained, and read as previously reported (Castrillón *et al*., 2019).

Statistical analysis

Data obtained from three independent experiments was reported as mean ± standard error (SE). One-way analysis of variance and Dunnett's test were used to evaluated statistical differences between treated cells and control group (nontreated). *p*-values lesser than 0.05 (typically ≤ 0.05) were considered statistically significant. To analyze experimental data, GraphPad Prism software V.7 for Windows was used.

Theoretical drug-likeness and pharmacokinetic indices

Ten biopharmaceutical relevant properties were screened for the most promising trihybrid **4j**. To that, MW, topographical polar surface area (TPSA), and rotatable bonds descriptors were calculated by using Molinspiration Chemoinfomatics Software. Meanwhile, human serum albumin ($LogK_{HSA}$), apparent predicted intestinal permeability (app. Caco-2 and MDCK models), and gastrointestinal uptake and absorption (%GI) were estimated using the online PreADMET 2.0 program. In addition, the ALOGPS 2.1 algorithm was used to calculate the lipophilicity parameter, log $P_{o/w}$.

RESULTS AND DISCUSSION

Chemistry

Novel salicylic acid/isoleucine/*N*-acylhydrazone (SA-Ile-NAH) hybrids were synthetized through a four-step (i–iv) divergent sequence of reactions shown in Scheme 1. To summarize, commercially available isoleucine as starting material was esterified to the corresponding methyl ester using thionyl chloride ($SOCl_2$) in methanol solvent by a modified Fischer esterification mechanism (Castrillón *et al*., 2019) to give ester **1** in quantitative yields, which was subjected to one-pot coupling procedure with available SA using HBTU as amide bond promoter and triethylamine (Et_3N) as a Lewis base to obtain **2** in good yields (71%) (Castrillón *et al*., 2019; Herrera *et al*., 2021). Subsequently, this intermediate reacted with hydrazine hydrate via nucleophilic substitution to obtain in high yield (93%) the desired *N*-acylhydrazide **3** (Coa *et al*., 2015; Vergara *et al*., 2017). Finally, the target SA-Ile-NAH hybrids **4a–l** were obtained in moderate to excellent yields (54%–94%) via Brønsted acid-catalyzed imine formation between the hydrazide **3** with the corresponding aromatic aldehydes (ArCHO) in ethanol under conditions of microwave heating, as described in Scheme 1 (Coa *et al*., 2015; Vergara *et al*., 2017). The structures of all compounds have been fully characterized by a combined ^{1}H-NMR and ^{13}C-NMR study with carbon atom types (C, CH, CH_2, and CH_3), determined by using the distortionless enhancement by polarization transfer or attached proton test pulse sequence. The signals were assigned using two-dimensional heteronuclear correlations (correlation spectroscopy and heteronuclear single quantum correlation). The ^{1}H-NMR spectra of hybrids **4a–l** dissolved in DMSO-d_6 showed a characteristic singlet peak within the 7.98–9.22 ppm range which is assigned to the proton of the azomethine group (-CH=N-). The isoleucine moiety was recognized by their two methyl groups which give a characteristic row of double signals within the 0.64–1.06 ppm range, while the signals corresponding to α-CH (~4.5 ppm) and CH_2 aliphatic protons were registered in the range of δ = 1.4–2.0 ppm. ^{1}H-NMR spectra also confirm the presence of aromatic protons which were located in the downfield region (6.70–8.60 ppm). Analysis of the ^{13}C NMR data for the **4a–l** hybrids showed a peak in the range of

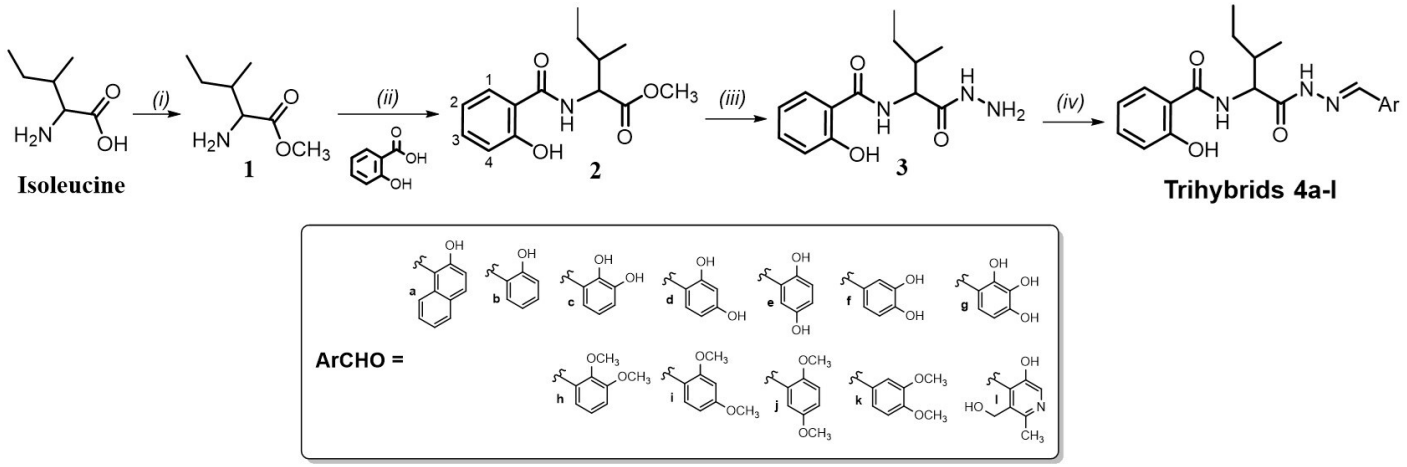

Scheme 1. Reagents and conditions: (i) $SOCl_2$, MeOH, 0°C; then rt, 48 hours, 95%. (ii) HBTU, Et_3N, THF, rt, 24 hours, 71%. (iii) $NH_2NH_2.H_2O$, 98%, MeOH, reflux, 24 hours, 93%. (iv) AcOH (cat), EtOH, reflux, 10 minutes, (µw), 54%–94%.

140–152 ppm which confirmed the presence of azomethine carbon in the hybrid structure. Moreover, the ^{13}C-NMR spectrum shows 5 signals in the 10–60 ppm upfield region, which was assigned to the carbon atoms of the aliphatic chain in the isoleucine portion. In addition, ^{13}C-NMR spectra of hybrids show two picks around 170 and 167 ppm, respectively, which confirms the presence of both carbonyl groups (C=O). Finally, aromatic carbons appear between 120 and 170 ppm. (see Supplementary Online Material for further details)

Biological activity

Cytotoxic effect of SA-Ile-NAH hybrids on SW480 and CHO-K1 cell lines

The cytotoxic effect of the synthesized *SA-Ile-NAH* hybrids using an *in vitro* model of human colorectal adenocarcinoma (SW480) and the nonmalignant CHO-K1 cell line were measured by the SRB colorimetric assay. In addition to the trihybrid compounds, 5-FU and the promising PIH were also included as positive controls, as well as the parent scaffolds SA and isoleucine and their equimolar mixture. Cytotoxicity data for the compounds are reported as half-maximal IC_{50} values and listed in Table 1.

In general, most trihybrids exhibited comparable cytotoxic activity to the reference drug 5-FU and PIH, being significantly more active than the parental subunits (SA and isoleucine) and their respective unlinked equimolar mixture, displaying promising *in vitro* cytotoxic effects in a concentration range of 20.43 ± 1.88 and 168.2 ± 20.33 µM after 48 hours of treatment. Furthermore, as can be seen in Table 1, most of those compounds increased the cytotoxic response over time as evidenced by the reduction in the IC_{50} values at 48 hours (see values at 24 *vs*. 48 hours). It is worth noting that the proposed molecular design allowed obtaining molecules with improved cytotoxic properties with respect to their respective parental compounds (SA and isoleucine), considerably higher activity than the equimolar mixture, and exhibited cytotoxic potency similar to that of 5-FU and PIH, thereby demonstrating a remarkable advantage of the molecular hybridization strategy.

Despite trihybrids **4a-c**, **4f**, **4h, 4i**, and **4l** improving the efficacy over malignant cells (SW480), a decrease in selectivity due to the high toxicity on nonmalignant cells (CHO-K1) was also observed after 48 hours of treatment. It was, however, observed that the 2,5-dimethoxy-substituited trihybrid **4j** highlighted not only for its good cytotoxic effect (IC_{50} = 78.15 ± 6.73 µM) but has no significant toxicity to nontumor cells (IS = 1.31). More importantly, a microscopic inspection (Fig. 2A and B) revealed that hybrid **4j** induced marked cell morphology changes related to the size and shape in SW480 colorectal cell line which is highly associated with cell death process, while a typical and healthy shape was observed after treatment with DMSO as control vehicle. Moreover, hybrid **4j** was able to induce a visible reduction in the total number of cells in a dose-dependent manner suggesting that this compound is able to induce a short-term loss of cell viability by either cytostatic or cytotoxic effect on tumor cells.

Table 1. Cytotoxic effect of SA-Ile-NAH hybrids against SW480 and CHO-K1 cell lines after 24 and 48 hours of treatment.

Hybrid compound	IC_{50} (µM) SW480 cells	24 hours		48 hours		
		IC_{50} (µM) CHO-K1 cells	SI	IC_{50} (µM) SW480 cells	IC_{50} (µM) CHO-K1 cells	SI
4a	54.20 ± 6.32	9.42 ± 1.46	0.17	20.43 ± 1.88 ****	2.54 ± 0.24	0.12
4b	278.00 ± 26.16	71.37 ± 6.66	0.26	143.30 ± 14.02	46.64 ± 3.51	0.33
4c	93.03 ± 8.93	112.40 ± 9.42	1.21	36.54 ± 2.82 ****	26.69 ± 1.40	0.70
4d	>500	236.30 ± 12.94	< 0.5	220.10 ± 22.49	126.90 ± 3.46	0.58
4e	>500	338.10 ± 29.11	< 1.0	370.80 ± 33.50	216.70 ± 12.69	0.58
4f	94.18 ± 10.32	78.94 ± 4.64	0.84	66.29 ± 5.86 ***	26.68 ± 2.94	0.40
4g	>500	210.40 ± 22.04	<0.5	>500	181.70 ± 15.56	<0.5
4h	115.90 ± 5.31	121.70 ± 9.72	1.05	80.79 ± 4.12 ****	78.63 ± 4.64	0.97
4i	166.70 ± 11.69	181.30 ± 2.90	1.09	150.10 ± 7.31 ***	160.10 ± 3.94	1.07
4j	106.00 ± 8.51	124.50 ± 7.34	1.17	78.15 ± 6.73 ***	102.40 ± 4.64	1.31
4k	272.20 ± 16.15	207.70 ± 11.43	0.76	185.60 ± 10.84	151.10 ± 2.52	0.81
4l	>500	142.50 ± 10.34	<0.5	168.20 ± 20.33	53.70 ± 2.72	0.32
SA	310.00 ± 32.76	NI	>1.0	>500	NI	>1
Isoleucine	284.50 ± 15.80	361.70 ± 31.86	1.27	>500	264.5 ± 12.2	< 0.5
SA + Isoleucine*	286.50 ± 36.49	>500	>1.0	>500	>500	>1
PIH**	281.40 ± 27.48	308.50 ± 34.71	1.10	111.60 ± 5.89	75.32 ± 6.44	0.67
5-FU	1,544.00 ± 127.90	543.50 ± 52.94	0.35	174. 30 ± 19.10	173.20 ± 14.61	0.96

IC_{50} values were obtained from dose–response curves for each compound at 48 hours. Data are presented as the mean ± SE of at least three independent experiments.
*Equimolar combination.
PIH. *p*-values lower than 0.05 were considered statistically significant. (*$p < 0.001$, ****$p < 0.0001$). Data are presented as the mean ± SE of at least three independent experiments. NI: No inhibition.

Studies of the SAR were conducted at 48 hours after incubation. Results revealed a synergistic action of the parent subunits when they are linked to form a single structure in the hybrid. Hybrid **4a** exhibited better cytotoxicity than compound **4b**, which shows the importance of the naphthyl group over the phenyl group for activity. The change of the phenyl group by the pyridyl group causes a slight decrease in the activity (**4b** *vs.* **4l**). The presence of a hydroxyl group at the C-3 position of the aromatic ring increased the activity (**4b** *vs.* **4c**). However, when this group changes position, the activity decreases (**4c** *vs.* **4d** and **4e**). Hybrid **4g**, a combination of compounds **4b** and **4f**, was not active, showing that there was no synergistic effect in SW480 cells, which was reflected in decreased activity compared to the initial hybrids (Fig. 3).

The methylation effect is not clear, because when the hybrids **4c** and **4h** are compared, it is possible to observe a decrease in activity. However, an opposite behavior is observed when the other hybrids are compared (**4d** *vs.* **4i** and **4e** *vs.* **4j**); in these cases, the activity increases. These findings are in good agreement with other reports, where compounds combining structural moieties of SA and hydrazone displayed a promising anticancer potential (Alam *et al*., 2017; Jongstra *et al*., 2006; Misko *et al*., 2019). Moreover, similar results were reported by Herrera *et al.* (2021) who also measured good cytotoxic and selective activity of hybrids of SA incorporating an S-allylcysteine fragment, using human colorectal adenocarcinoma SW480 cell lines as model. We hypothesized that the cytotoxic effect on SW480 cells observed after SA-Ile-NAH hybrids exposure could be associated to the fact that these compounds would be able to target essential bioreceptors through formation of intermolecular hydrogen bonds, oxidative stress triggered by reactive free-radical species formation, and/or the ability of metal complexation. However, further experimental and computational investigations need to be conducted in order to elucidate the most plausible antiproliferative mechanism of these promising trihybrids. According to the aforementioned findings, merging SA, isoleucine, and hydrazone moieties into a unique structural core provides promising compounds that could be considered a novel interesting therapeutical scaffold for developing new antitumoral compounds, particularly in CRC. In addition, further investigations by introducing electron-withdrawing substituents and electron-donating core combinations in the aromatic ring attached to the hydrazone moiety will be conducted aiming at improving the selectivity of most of the tested compounds. Studies of how these electronics effects can affect the antiproliferative potency, not only in CRC but other most commonly diagnosed cancers at even higher risk, are also needed.

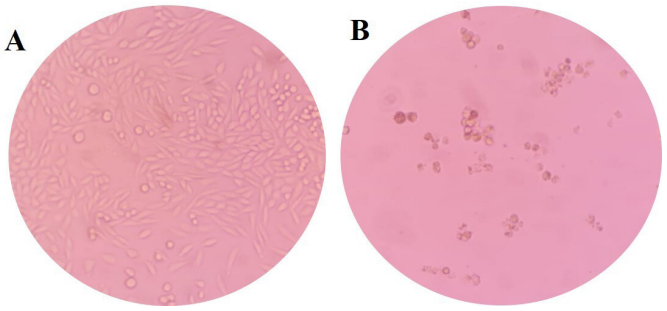

Figure 2. Images of growth control of SW480 cancer cell line (magnification: 20×). (A). Vehicle control. (DMSO) treatment. (B). After hybrid **4j** exposure (48 hours posttreatment)

Antiproliferative effect of 4j on SW480 cells

The antiproliferative effect of the most promising compound **4j** highlighted by the selectivity and cytotoxic effect was further evaluated to know if it can preserve its activity against SW480 cells after periods of time ranging from 2 to 8 days of treatment (Table 2).

To achieve this goal, SW480 adenocarcinoma cells were treated with increasing concentrations of 6.25, 12.5, 25, 50, and

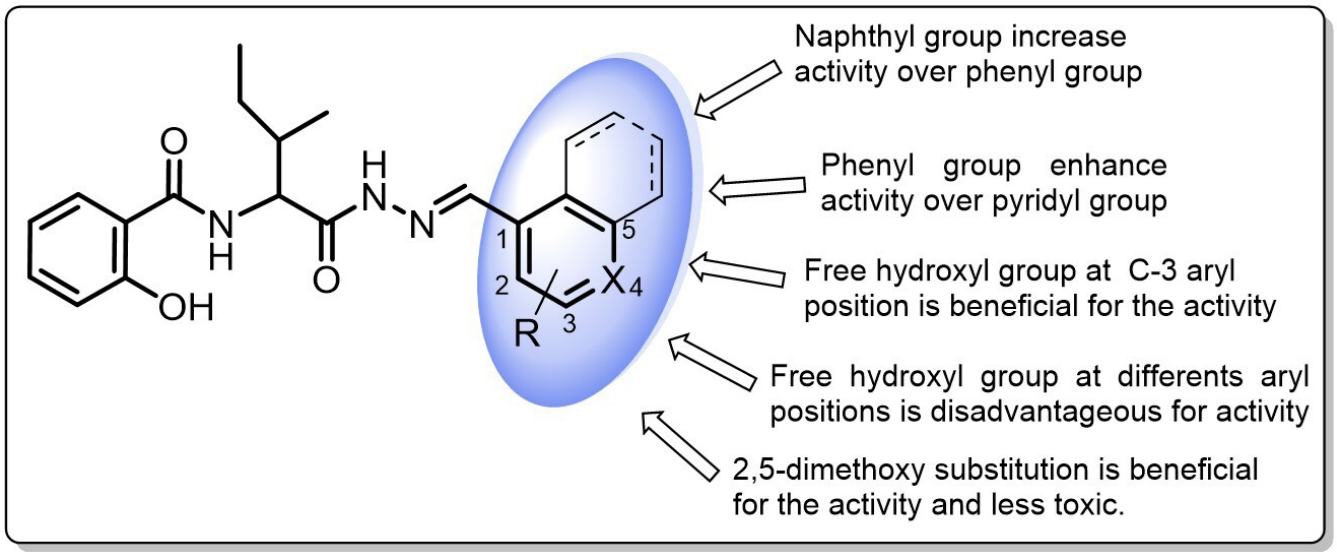

Figure 3. SAR for the cytotoxic activity of the novel SA-Ile-NAH hybrid.

Table 2. Data viability (%) of the five concentrations evaluated against SW480 cell.

Compound	Concentration (μM)	Time after plating (days)			
		2	4	6	8
		Viability (%) ± SE			
Hybrid 4j	6.25	86.10 ± 3.92	85.33 ± 2.38	80.93 ± 2.83	76.71 ± 3.83
	12.5	68.46 ± 3.72	33.91 ± 0.41	13.25 ± 0.83	11.14 ± 0.22
	25	65.56 ± 2.95	28.05 ± 1.07	9.55 ± 0.50	8.06 ± 0.25
	50	43.18 ± 3.55	9.93 ± 1.03	2.54 ± 0.29	0.69 ± 0.01
	100	33.97 ± 3.92	4.41 ± 0.42	0.72 ± 0.23	0.15 ± 0.01

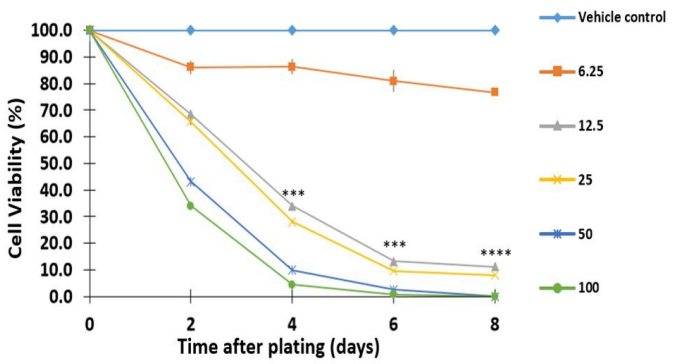

Figure 4. Antiproliferative effect of hybrid **4j** against SW480 cell line; Data are presented as the mean ± SE of at least three independent experiments (*$p < 0.05$; **$p < 0.01$; ***$p < 0.001$; ****$p < 0.0001$). Vehicle control was assumed as 100% viable.

100 μM of **4j** for 8 days and the cell viability was measured by the colorimetric SRB assay. As shown in Figure 4, our results in comparison with the control showed that trihybrid **4j** inhibited the proliferation of human colorectal adenocarcinoma cells (SW480), in dose- and time-dependent manner. Thus, treatment of tumor cells with **4j** reduced the number of viable cells and prevented the exponential growth of the primary tumor cell line examined. Particularly, after 4 days of treatment with 25–100 μM, this hybrid significantly reduced the viability of the SW480 cells compared to untreated control cells, with *p*-values lesser than 0.001. Notably, when SW480 cells were treated with a low concentration of **4j (**12.5 μM), the number of tumor cell colonies was also significantly reduced within 4 days of treatment. All these findings demonstrated that hit compound **4j** caused a time- and dose-dependent loss of SW480 cell viability confirming the previous results of viability and suggesting that trihybrid **4j** may *in vitro* induce either cytostatic/cytotoxic response on the colon cancer cell line model. We conclude here that, the synthetized SA-Ile-NAH hybrids compounds, particularly compound **4j**, emerge as attractive building blocks in the search of new anti-CRC agents.

Theoretical pharmacokinetic and drug-likeness properties of promising trihybrid 4j

Drug-likeness and pharmacokinetics inspections represent a valuable strategy to complete the journey from initial discovery to the marketplace of novel drug candidates in pharmaceutical research, particularly in assessing the quality of novel antitumor scaffolds. Here, for the most promising trihybrid **4j,** we have predicted 10 biopharmaceutical indices that have the most profound influence on drug-like properties of a molecule, such as molecular weight, polar surface area, number of hydrogen bond acceptors/donors, octanol–water partition coefficient, binding-serum albumin, human intestinal permeation (Caco-2 and MDCK cells models), and a number of rotatable bonds. The drug-likeness and pharmacokinetic predictions provided by the SwissADME and pre-ADMET software are listed in Table 3. Our results show that a favorable pharmacokinetics profile was found for the examined hybrid when compared to 95% of oral U.S. Food and Drug Administration-marketed drugs. **4j** did not violate any of Lipinski's rule of five (Lipinski *et al*., 1997). Moreover, the degree of lipophilicity (expressed as $LogP_{o/w}$) was in good agreement with the optimal quality parameters for oral lipid-based formulations (–2.0 to 6.0) (Ditzinger *et al*., 2019). Furthermore, **4j** displayed an optimal human intestinal absorption (%GI) number larger than 80%, and good predicted permeability data in the range of 536–1,077 nm/second when traditional Caco-2 and MDCK cells models were used, respectively (Broccatelli *et al*., 2016; Pham-The *et al*., 2018; Press and Di Grandi, 2008). Meanwhile, the compound exhibits a computational TPSA value of 106.75 $Å^2$ within the ideal value of less than 140 $Å^2$ (Ertl *et al*., 2000). We predict that **4j** would bind favorably to human serum albumin (expressed as $logK_{HSA}$), within the recommended therapeutic range suggested for potential drug candidates (–1.5 to 1.5) (Colmenarejo, 2003; Zhivkova, 2015). Finally, the pan-assay interference compounds (PAINS) filter, which provides early alerts for potential toxicity as part of successful drug discovery, showed that the promising **4j** hybrid can be regarded as valid starting points in cancer drug discovery.

Taken altogether, merging salicylic acid, *N*-acylhydrazone, and isoleucine scaffolds into a new single chemical structure

Table 3. Lipinski's rule and pharmacokinetic indices for the hit compound **4j.**

Properties	4j	Properties [j]	4j
MW [a]	413.47	Log S [k]	-4.52
TPSA [b]	106.75	BBB permeant [l]	No
n-Rot Bond	10	PAINS [m]	0
n-ON [c]	6	MR [n]	114.46
n-OHNH [d]	2	CYP1A2 inhibitor [o]	No
Log $P_{o/w}$ [e]	4.82	CYP2D6 inhibitor [p]	No
$LogK_{HSA}$ [f]	0.631	CYP3A4 inhibitor [q]	No
Caco-2 (nm/s) [g]	1,077	NHA [r]	30
App. MDCK (nm/s) [h]	536	Synthetic accessibility	3.99
% GI [i]	>80%	P-gp substrate [s]	Yes
Lipinski's violations (≤1)	0		

[a] Molecular weight of the compound (150–500).
[b] Total polar surface area (*TPSA*) (<140 $Å^2$).
[c] *n-ON* number of hydrogen bond acceptors <10.
[d] n-*OHNH* number of hydrogens bonds donors ≤5.
[e] Octanol–water partition coefficient ($log\ P_{o/w}$) (−2.0 to 6.5).
[f] Binding-serum albumin ($LogK_{HSA}$) (−1.5 to 1.2).
[g] Human intestinal permeation (<25 poor and >500 great).
[h] Madin–Darby canine kidney (*MDCK*) cells permeation (<25 poor and >500 great).
[i] % Human oral gastrointestinal (*GI*) absorption >80%, high; <25%, poor.
[j] Calculated using the login-free SwissADME online tool (http://www.swissadme.ch.).
[k] Aqueous solubility; logS = log (g/100 g water); insoluble < −10 < Poorly < −6 < Moderately < −4 < Soluble < −2 Very < 0 < Highly.
[l] The blood–brain barrier (BBB) permeation.
[m] Identification of potentially problematic fragments for PAINS.
[n] Molar refractivity (40–130).
[o] Inhibition of cytochrome P450 1A2.
[p] Cytochrome P-450 CYP2D6 inhibition.
[q] Cytochrome P450 3A4 inhibition.
[r] Number of heavy atoms (5–40).
[s] P-glycoprotein binding (transport across extra- and intracellular membranes).
SUPPLEMENTARY MATERIAL
^1H and ^{13}C NMR spectra of the intermediate compounds **1–3** as well as target hybrids **4a–l** are provided in the supporting in formation .

provides bioactive compounds with an optimal pharmacokinetic profile. Accordingly, novel trihybrid scaffolds based on SA-Ile-NAH should be taken into account for further investigations focused on the design of new oral antitumoral drug candidates to combat CRC**.**

CONCLUSION

A novel series of SA-Ile-NAH trihybrids was designed, synthesized, and screened for cytotoxic effect on SW480 human colon adenocarcinoma cells. Most of these hybrids were more potent than the reference drug (5-FU) and the equimolar mixture as well as than the parental subunits (SA and isoleucine). In particular, the 2,5-dimethoxy-substituited trihybrid **4j** was the most promising compound because it not only displayed good cytotoxic potency against SW480 human colon cancer cells, but also expressed remarkable antiproliferative activity at lower concentrations, and no significant toxic effects on nontumorigenic cells. Moreover, **4j** showed an optimal drug-likeness/pharmacokinetic profile. Considering all these results, trihybrids based on SA-Ile-NAH emerge as a promising therapeutic opportunity against CRC in the forthcoming years.

FUNDING

This work was financially supported by Universidad de Antioquia through the Committee for Research Development (Comité para el Desarrollo y la Investigación) CIEN–CODI–Vicerrectoría de Investigación (Primer proyecto), project number 2018-21112.

CONFLICT OF INTEREST

The authors declare that there is no conflict of interest.

ETHICAL APPROVAL

This study does not involve the use of animals or human subjects.

AUTHOR CONTRIBUTIONS

All authors made substantial contributions to conception and design, acquisition of data, or analysis and interpretation of data; took part in drafting the article or revising it critically for important intellectual content; agreed to submit to the current

journal; gave final approval of the version to be published; and agree to be accountable for all aspects of the work. All the authors are eligible to be an author as per the international committee of medical journal editors (ICMJE) requirements/guidelines

DATA AVAILABILITY

All data generated and analyzed are included within this research article.

PUBLISHER'S NOTE

This journal remains neutral with regard to jurisdictional claims in published institutional affiliation.

REFERENCES

Alam MS, Choi SU, Lee DU. Synthesis, anticancer, and docking studies of salicyl-hydrazone analogues: A novel series of small potent tropomyosin receptor kinase A inhibitors. Bioorg Med Chem, 2017; 25(1):389–96.

Al-awar R, Mamai A, Zhang A, inventors. Acyl hydrazone linkers, methods and uses thereof. WO2019109188A1, 2019 June 13.

Ali I, Wani WA, Haque A, Saleem K. Glutamic acid and its derivatives: candidates for rational design of anticancer drugs. Future Med Chem, 2013; 5(8):961–78.

Ananieva EA, Wilkinson AC. Branched-chain amino acid metabolism in cancer. Curr Opin Clin Nutr Metab Care, 2018; 21(1):64–70.

Bagheri M, Hesari A, Sarabi P, Rahimi H, Baazm M, Ghasemi F. Antiproliferative effect of aspirin on colorectal cancer cell line. Iran J Tox, 2018; 12(5):1–4.

Bener A, Dogan M, Azab A, Rashed A, Siddiqui M. Short communication: amino acid profiles among colorectal cancer patients. Biomed Res, 2006; 17(2):149–54.

Brennan CA, Nakatsu G, Gallini Comeau CA, Drew DA, Glickman JN. Aspirin modulation of the colorectal cancer-associated microbe *Fusobacterium nucleatum*. mBio, 2021; 12(2):e00547–21.

Broccatelli F, Salphati L, Plise E. Predicting passive permeability of drug-like molecules from chemical structure: where are we? Mol Pharm, 2016; 13(12):4199–208.

Burn J, Sheth H, Elliott F, Reed L, Macrae F, Mecklin JP. Cancer prevention with aspirin in hereditary colorectal cancer (Lynch syndrome), 10-year follow-up and registry-based 20-year data in the CAPP2 study: a double-blind, randomised, placebo-controlled trial. Lancet, 2020; 395(10240):1855–63.

Buss JL, Hermes-Lima M, Ponka P. Pyridoxal isonicotinoyl hydrazone and its analogues. Adv Exp Med Biol, 2002; 509:205–29.

Castrillón W, Herrera-R A, Prieto LJ, Conesa-Milián L, Carda M, Naranjo T, Maldonado ME, Cardona-G W. Synthesis and *in-vitro* evaluation of *S*-allyl cysteine ester-caffeic acid amide hybrids as potential anticancer agents. Iran J Pharm Res, 2019; 18(4):1770–89.

Chaston TB, Lovejoy DB, Watts RN, Richardson DR. Examination of the antiproliferative activity of iron chelators: multiple cellular targets and the different mechanism of action of triapine compared with desferrioxamine and the potent pyridoxal isonicotinoyl hydrazone analogue 311. Clin Cancer Res, 2003; 9(1):402–14.

Chen YL, Kong X, Xie Y, Hider RC. The interaction of pyridoxal isonicotinoyl hydrazone (PIH) and salicylaldehyde isonicotinoyl hydrazone (SIH) with iron. J Inorg Biochem, 2018; 180:194–203.

Coa JC, Castrillón W, Cardona W, Carda M, Ospina V, Muñoz JA, Vélez ID, Robledo SM. Synthesis, leishmanicidal, trypanocidal and cytotoxic activity of quinoline-hydrazone hybrids. Eur J Med Chem, 2015; 101:746–53.

Colmenarejo G. In silico prediction of drug-binding strengths to human serum albumin. Med Res Rev, 2003; 23(3):275–301.

Cuzick J, Otto F, Baron JA, Brown PH, Burn J, Greenwald P. Aspirin and non-steroidal anti-inflammatory drugs for cancer prevention. Lancet Oncol, 2009; 10(5):501–7.

Dasgupta S, Karim S, Banerjee S, Saha M, Das Saha K, Das D. Designing of novel zinc(ii) Schiff base complexes having acyl hydrazone linkage: study of phosphatase and anti-cancer activities. Dalton Trans, 2020; 49(4):1232–40.

Deb J, Dibra H, Shan S, Rajan S, Manneh J, Kankipati CS. Activity of aspirin analogues and vanillin in a human colorectal cancer cells. Oncol Rep, 2011; 26(3):557–65.

Delphan M, Lin T, Liesenfeld DB, Nattenmüller J, Böhm JT, Gigic B. Associations of branched-chain amino acids with parameters of energy balance and survival in colorectal cancer patients: results from the ColoCare Study. Metabolomics, 2018; 2018(14):22–31.

Ditzinger F, Price DJ, Ilie AR, Köhl NJ, Jankovic S, Tsakiridou G. Lipophilicity and hydrophobicity considerations in bio-enabling oral formulations approaches—a PEARRL review. J Pharm Pharmacol, 2019; 71:464–82.

Elder DJ, Hague A, Hicks DJ, Paraskeva C. Differential growth inhibition by the aspirin metabolit salicylate in human colorectal tumor cell lines. Cancer Res, 1996; 56(10):2273–6.

Elder DJ, Paraskeva C. Induced apoptosis in the prevention of colorectal cancer by non-steroidal anti-inflammatory drugs. Apoptosis, 1999; 4(5):365–72.

Ertl P, Rohde B, Selzer P. Fast calculation of molecular polar surface area as a sum of fragment-based contributions and its application to the prediction of drug transport properties. J Med Chem, 2000; 43(20):3714–7.

Ferlay J, Ervik M, Lam F, Colombet M, Mery L, Piñeros M. Global cancer observatory: cancer today. International Agency for Research on Cancer, Lyon, France, 2020. Availabel via https://gco.iarc.fr/today (Accessed 1 February 2022).

Giardina C, Inan MS. Nonsteroidal anti-inflammatory drugs, short-chain fatty acids, and reactive oxygen metabolism in human colorectal cancer cells. Biochim Biophys Acta, 1998; 1401(3):277–88.

GLOBOCAN. Cancer incidence and mortality, 2020. Available via https://www.uicc.org/news/globocan-2020-new-global-cancer-data (Accessed 19 April 2021).

Gökçe K, İşkan N, Türker N, Kaşit M. Evaluating combined effect of naringin and salicylic acid on colon cancer cell culture. Turkish Med Stud J, 2017; 4:17–24

Herrera A, Castrillón W, Otero E, Ruiz E, Carda M, Agut R. Synthesis and antiproliferative activity of 3- and 7-styrylcoumarins. Med Chem Res, 2018; 27:1893–905.

Herrera-R A, Castrillón W, Pastrana M, Yepes AF, Cardona-G W. Promising hybrids derived from S-allylcysteine and NSAIDs fragments against colorectal cancer: synthesis, in-vitro evaluation, drug-likeness and in-silico ADME/tox studies. Iran J Pharm Res, 2021; (3):351–67.

Høydahl Ø, Edna TH, Xanthoulis A, Lydersen S, Endreseth BH. Long-term trends in colorectal cancer: incidence, localization, and presentation. BMC Cancer, 2020; 20(1):1077–90.

Huff SE, Mohammed FA, Yang M, Agrawal P, Pink J, Harris ME. Structure-guided synthesis and mechanistic studies reveal sweetspots on naphthyl salicyl hydrazone scaffold as non-nucleosidic competitive. J Med Chem, 2018; 61(3):666–80.

Iliev I, Kontrec D, Detcheva R, Georgieva M, Balacheva A, Galic N. Cancer cell growth inhibition by aroylhydrazone. Biotechnol. Biotec. Equip, 2019; 33(1):756–63.

Jongstra J, Kotra LP, Wrana JL, inventors. Salicylic acid hydrazones as inhibitors of the erk mapkinase for the treatment of cancer. WO 2006136008 A1, 2006, December 28.

Lieu EL, Nguyen T, Rhyne S. Amino acids in cancer. Exp Mol Med, 2020; 52:15–30.

Lipinski CA, Lombardo F, Dominy BW, Feeney PJ. Experimental and computational approaches to estimate solubility and permeability in drug discovery. Adv Drug Deliv Rev, 1997; 23:3–25.

Long L, Yang W, Liu L, Tobias DK, Katagiri R, Wu K. Dietary intake of branched-chain amino acids and survival after colorectal cancer diagnosis. Int J Cancer, 2020; 148(10):2471–80.

Misko TA, Liu YT, Harris ME, Oleinick NL, Pink J, Lee HY. Structure-guided design of anti-cancer ribonucleotide reductase inhibitors. J Enzyme Inhib Med Chem, 2019; 34(1):438–50.

Murata K, Moriyama M. Isoleucine, an essential amino acid, prevents liver metastases of colon cancer by antiangiogenesis. Cancer Res, 2007; 67(7):3263–8.

Paterson JR, Lawrence JR. Salicylic acid: a link between aspirin, diet and the prevention of colorectal cancer. QJM, 2001; 94(8):445–48.

Pathi S, Jutooru I, Chadalapaka G, Nair V, Lee SO, Safe S. Aspirin inhibits colon cancer cell and tumor growth and downregulates specificity protein (Sp) transcription factors. PLoS One, 2012; 7(10):e48208–17.

Patrignani P, Patrono C. Aspirin and cancer. J Am Coll Cardiol, 2016; 68(9):967–76.

Peleg II, Maibach HT, Brown SH, Wilcox CM. Aspirin and nonsteroidal anti-inflammatory drug use and the risk of colorectal cancer. Arch Intern Med, 1994; 154(4):394–99.

Perez J, Maldonado M, Rojano B, Alzate F, Saez J, Cardona W. Comparative Antioxidant, Antiproliferative and Apoptotic effects of Ilex laurina and Ilex paraguariensis on Colon Cancer Cells Trop J Pharm Res, 2014; 13(8):1279–86.

Pham-The H, Cabrera-Pérez MÁ, Nam NH, Castillo-Garit JA, Rasulev B, Le-Thi-Thu H, Casañola-Martin GM. In Silico Assessment of ADME properties: advances in Caco-2 cell monolayer permeability modeling. Curr Top Med Chem, 2018; 18(26):2209–29.

Press B, Di Grandi D. Permeability for intestinal absorption: Caco-2 assay and related issues. Curr Drug Metab, 2008; 9(9):893–900.

Siegel RL, Miller KD, Fuchs HE, Jemal A. Cancer statistics, 2021. CA Cancer J Clin, 2021; 71:7–33.

Song S, Christova T, Perusini S, Alizadeh S, Bao RY, Miller BW. Wnt inhibitor screen reveals iron dependence of β-catenin signaling. Cancer Res, 2011; 71(24):7628–39.

Spiegel R. Aspirin as a painkiller in patients with a high cardiovascular risk profile. Nat Rev Cardiol, 2020; 17(9):609–19.

Sung H, Ferlay J, Siegel RL, Laversanne M, Soerjomataram I, Jemal A, Bray F. Global cancer statistics 2020: GLOBOCAN estimates of incidence and mortality worldwide for 36 cancers in 185 countries. CA Cancer J Clin, 2021; 71:209–49.

Thota S, Rodrigues DA, Pinheiro PSM, Lima LM, Fraga CAM. N-Acylhydrazones as drugs. Bioorg Med Chem Lett, 2018; 28(17):2797–306.

Thun MJ, Namboodiri MM, Heath CW Jr. Aspirin use and reduced risk of fatal colon cancer. N Engl J Med, 1991; 325(23):1593–96.

Vergara S, Carda M, Agut R, Yepes LM, Robledo SM, Cardona W. Synthesis, antiprotozoal activity and cytotoxicity in U-937 macrophages of triclosan–hydrazone hybrids. Med Chem Res, 2017; 26:3262–73.

Viegas-Junior C, Danuello A, da Silva Bolzani V, Barreiro EJ, Fraga CA. Molecular hybridization: a useful tool in the design of new drug prototypes. Curr Med Chem, 2007; 14(17):1829–52.

Wakshlag JJ, Kallfelz FA, Wakshlag RR, Davenport GM. The effects of branched-chain amino acids on canine neoplastic cell proliferation and death. J Nutr, 2006; 136(7):2007–10.

Wang LB, Zhang SZ, Ding KF, Zheng S. A study of the free amino acids uptake in Colon Cancer. Zhejiang Y, 1997; 19:208–9.

Zhivkova ZD. Studies on drug-human serum albumin binding: the current state of the matter. Curr Pharm Des, 2015; 21(14):1817–30.

SUPPLEMENTARY MATERIAL

^{1}H and ^{13}C NMR spectra of the intermediate compounds **1–3** as well as target hybrids **4a–l** are provided in the supporting information.

How to cite this article:
Preciado D, Moreno G, Cardona W, Yepes AF. Discovery of novel trihybrids based on salicylic acid/isoleucine/*N*-acylhydrazone: A promising therapeutic opportunity in colorectal cancer. J Appl Pharm Sci, 2022; 12(11):010–020.